Spin density wave instabilities in the NbS_2 monolayer

F. Güller,[1,2] V. L. Vildosola,[1,2] and A. M. Llois[1,2,3]

[1]*Centro Atómico Constituyentes, GIyANN, CNEA, Avenida General Paz 1499, San Martín, Buenos Aires, Argentina*

[2]*Consejo Nacional de Investigaciones Científicas y Técnicas, Avenida Rivadavia 1917 (C1033AAJ), Buenos Aires, Argentina*

[3]*Departamento de Física Juan José Giambiagi, FCEyN-UBA, Intendente Güiraldes 2160 (C1428EGA), Buenos Aires, Argentina*

(Received 21 October 2015; revised manuscript received 5 January 2016; published 29 March 2016)

In the present work, we study the magnetic properties of the NbS_2 monolayer by first-principles calculations. The transition metal dichalcogenides (TMDCs) are a family of laminar materials presenting exciting properties such as charge density waves (CDWs), superconductivity, and metal-insulating transitions. $2H$-NbS_2 is a particular case within the family, because it is the only one that is a superconductor without exhibiting a CDW order. Although no long-range magnetic order was experimentally observed in the TMDCs, we show here that the single monolayer of NbS_2 is on the verge of a spin density wave (SDW) phase. Our calculations indicate that a wavelike magnetic order is stabilized in the NbS_2 monolayer in the presence of magnetic defects or within zigzag nanoribbons, due to the presence of unpaired electrons. We calculate the real part of the bare electronic susceptibility and the corresponding nesting function of the clean NbS_2 monolayer, showing that there are strong electronic instabilities at the same wave vector associated with the calculated SDWs, also corresponding with one of the main nesting vectors of the Fermi surface. We conclude that the physical mechanism behind the spin-wave instabilities are the nesting properties, accentuated by the quasi-2D character of this system, and the rather strong Coulomb interactions of the 4*d* band of the Nb atom. We also estimate the amplitude of the spin fluctuations and find that they are rather large, as expected for a system on the verge of a quantum critical transition.

DOI: 10.1103/PhysRevB.93.094434

I. INTRODUCTION

Transition metal dichalcogenides (TMDCs), MX_2 ($X = $ S, Se, or Te), constitute a family of compounds with fascinating physical properties such as charge-ordered phases and superconductivity. They are characterized by a laminar structure similar to that of graphite. Each monolayer is actually a trilayer, composed by a plane of metal atoms sandwiched by two planes of S, Se, or Te. Within one trilayer, the atoms are covalently bound while separate trilayers are held together mainly through weak van der Waals interactions. In pristine TMDCs there are two different bulk structures (polytypes), abbreviated by $1T$ and $2H$, corresponding to the either octahedral or trigonal prismatic coordination of the M atom. The primitive cell of the $1T$ and $2H$ polytypes contains one and two monolayers, respectively.

Bulk TMDCs can present strikingly different behaviors depending on the polytype. For instance, charge density wave (CDW) transitions occur in both $1T$ and $2H$ structures but with very different structural and electronic properties. Some $1T$ systems are Mott insulators while in the $2H$ family there is no trace of Mott physics. In particular, the $2H$-MX_2 can be either metallic [such as $Nb(S,Se)_2$ and $Ta(S,Se)_2$] or band insulators (such as MoS_2 and WS_2), depending on the filling of the d band. Notably, also both polytypes can present a superconducting state. Many works have been devoted to studying the driving force of the CDW and its relation to superconductivity (SC). Naturally, the quasi-two-dimensional structure of these laminar materials is prone to a nesting scenario characterized by parallel pieces of the Fermi surface at a given "nesting" vector, $\mathbf{q_n}$. The traditional understanding would be that under this nesting condition, the electron system might become unstable and induce a CDW transition in the Peierls-like manner and/or a SDW one. However, it has been shown for $2H$-$NbSe_2$ and $2H$-$TaSe_2$, two prototypes of CDW systems, both by angle-resolved photoemission experiments (ARPES) and *ab initio* calculations, that the charge-ordering wave vector, q_{CDW}, is different from q_n, indicating that a simple nesting model [1,2] cannot account for the CDW in these materials. Instead, an enhancement of the electron-phonon coupling at q_{CDW} has been proposed to be the driving force. More recently, ARPES data supported by theoretical calculations of the k-resolved susceptibility suggested that the CDW instability is dominated by finite energy transitions from states far away from the Fermi surface. In any case, the general consensus is that the CDW in these systems is not of pure electronic origin [3].

Among the TMDCs, $2H$-NbS_2 is a particular case, because it is a superconductor like $2H$-$NbSe_2$, with a similar T_c, but no CDW ordering has been observed experimentally. First-principles calculations have shown that the CDW is suppressed in this material due to anharmonic effects [4]. These results suggest that since the superconducting properties are very similar to those of the isoelectronic $2H$-$NbSe_2$, either the nature of the ordered phase is not relevant for the superconducting state or there are other types of instabilities unexplored up to now. As was recently reviewed in Refs. [5,6], the TMDCs present many properties that are similar to the ones observed in the unconventional cuprates and Fe-based superconductors; a pseudogap behavior is one of them. However, no SDW or any other kind of long-range magnetic order has been observed in any of these TMDCs until now.

Experimentally, exfoliation techniques used to obtain graphene have been adjusted to TMDCs to produce analogous samples of lower dimensionality, be they a few monolayers, a single monolayer, and even nanoribbons or flakes. Another way to lower the dimensionality in TMDCs is through the intercalation with organic molecules or transition metals. Interestingly, it has been very recently observed, through

 ©2016 American Physical Society

optical and electrical transport measurements, that CDW effects in $NbSe_2$ are strongly enhanced in monolayers [7].

The fact that Nb is a 4*d* transition metal with important electronic exchange interactions and the feasibility of lowering the dimensionality of this type of laminar system motivated us to study the electronic properties of the NbS_2 monolayer. The absence of CDW order makes NbS_2 particularly appealing due to this relative simplicity.

In a previous work, we have shown by means of *ab initio* calculations that NbS_2 zigzag nanoribbons of different widths develop a wavelike pattern in their magnetic moments [8]. In the present work, we generalize the study of the magnetic instabilities and gain insight into the physical mechanism that drives the observed magnetic solutions. By calculating the real part of the bare electronic susceptibility in the constant matrix element approximation [9] and the corresponding nesting function we show that the nesting properties of the NbS_2 monolayer, together with the rather strong Coulomb exchange interaction of the 4*d* band, put this system to be on the verge of the SDW transition. As expected for a system close to a quantum critical magnetic transition, there should exist large spin fluctuations. We have estimated the amplitude of these fluctuations through the fluctuation-dissipation theorem obtaining a value that is consistent with this scenario. We reinforce this picture by showing that doping, defects, or ribbon edges can stabilize spin density waves in NbS_2 monolayers.

The paper is organized as follows. In Sec. II we describe the computational details. In Sec. III we study the electronic properties of the NbS_2 monolayer and the magnetic solutions that are obtained when placing defects or creating ribbon edges. We then analyze the static bare susceptibility of the monolayer and show the wavelike magnetic patterns to be SDW states. The estimation of the spin fluctuations of this system are described at the end of this section. Finally, we present our conclusions in Sec. IV.

II. COMPUTATIONAL DETAILS

Previous works have shown that *ab initio* calculations based on density functional theory (DFT) correctly describe the CDW phase in several $2H$-MX_2 (see for example Refs. [10–13]). In this work, to study the magnetic properties of the NbS_2 monolayer, the calculations were preformed using both the VASP [14–16] and WIEN2k [17,18] codes. The cross-check is particularly necessary in the case of the pristine NbS_2 monolayer since, as will be shown below, there are several competing phases very close in energy. For the exchange correlation potential the generalized gradient approximation as parametrized by Perdew *et al.* [19] was employed. The atom positions were modified until all forces were smaller than 0.02 eV/Å. To model the monolayers, a supercell with 13 Å vacuum in the perpendicular direction was used in order to avoid interactions between monolayers since periodic boundary conditions were applied in all directions. The *k*-point grid in the first Brillouin zone was $23\times23\times1$. For calculations of the Fermi surface and susceptibility it was enlarged to $200\times200\times1$, and an 8 meV Fermi temperature smearing was used. Only the VASP code was employed to analyze nanoribbons, which were simulated using a supercell with a 20 Å vacuum region in the two perpendicular directions. The *k*-point grid in these cases was $35\times1\times1$. We perform spin-polarized (SP) and non-SP calculations, with and without considering the spin-orbit interaction (SO), and discuss its effects in the results obtained.

III. RESULTS

To our knowledge, the experimental structural parameters of the hexagonal NbS_2 monolayer have not been reported yet. The available data correspond to bulk samples [20]. The obtained structural parameters, a and zc (zc being the height of the S atom relative to the Nb plane), of the relaxed NbS_2 monolayer are very close to the ones measured in the bulk. The relaxed monolayer has a slightly larger lattice constant a and a small increase of zc. The obtained values are $a = 3.34$ Å and $zc = 1.56$ Å, which are within 1% and 5% of the experimental ones for the bulk, respectively [21].

The most stable solution for the NbS_2 monolayer, both with and without SO coupling, is the non-SP one, if the calculations are carried out in the primitive cell (1×1). There is also a ferromagnetic phase, very close in energy, with 0.3 μ_B/Nb and 0.4 μ_B/Nb, with and without SO, respectively. The corresponding band structure (without SO) is shown in Fig. 1(a). There are six full S *p*-type bands, one band crossing the Fermi level of mainly Nb-d_{z^2} character (A_1' of the D_{3h} group) and four empty Nb-*d* bands with E' and E'' symmetries. Due to the strong covalency of this material, there is a strong *p*-*d* hybridization effect between the full and empty bands. In Fig. 1(b) we show the corresponding Fermi surface and the first Brillouin zone. One of the main nesting vectors is in the ΓM direction, indicated by arrows joining parts of the Fermi surface.

When a larger supercell is considered, nontrivial magnetic configurations appear. We study here a 4×4 supercell and observe that a wavelike pattern in the magnetic moments of the Nb atoms, shown schematically in Fig. 2(a), competes in energy with the non-SP solution. When using the WIEN2k code, without SO, the obtained wavelike configuration is energetically more favorable (by 2 meV/Nb) than the non-SP case. The maximum value of the magnetic moments is 0.4 μ_B/Nb. However, when the SO coupling is included in the calculation, the non-SP solution becomes more stable than the wavelike magnetic one with an energy difference

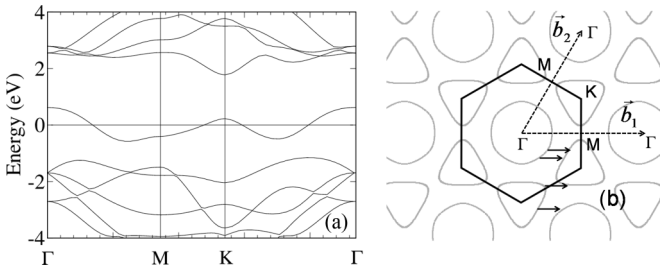

FIG. 1. (a) Non-SP band structure of the NbS_2 monolayer, without SO. The single band crossing the Fermi level (zero energy) is primarily of Nb-d_{z^2} character. (b) Corresponding Fermi surface of the NbS_2 monolayer. The first Brillouin zone is drawn in the center of the plot. $\mathbf{b_1}$ and $\mathbf{b_2}$ are the reciprocal lattice primitive vectors. One of the main nesting vectors is indicated by arrows.

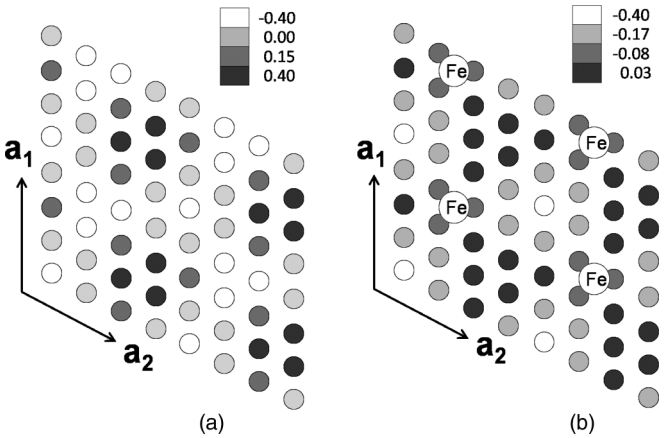

FIG. 2. Schematic representation of the magnetic moments (without SO) of the Nb atoms in a 4×4 supercell. All values, in μ_B, are approximate and intended as a guide for the eyes only. (a) Wavelike configuration that competes in energy with the non-SP solution in pristine NbS_2. (b) Configuration obtained with a single Fe adsorption. The Fe atom has a magnetic moment of $-2.6\ \mu_B$. $\mathbf{a_1}$ and $\mathbf{a_2}$ are the lattice primitive vectors and the 4×4 supercell is repeated twice along each direction.

of 4 meV/Nb. The energetics obtained with VASP is similar except for the fact that one can also find an intermediate, nearly degenerate ferromagnetic state, less than 1 meV/Nb from the non-SP one. The magnetic moments in the ferromagnetic case are 0.16 μ_B/Nb. It is important to remark that all the solutions are very close in energy and the values of the magnetic moments are highly dependent on the atomic positions and lattice constants. Also, the shape of the magnetic patterns is constrained by the periodic boundary condition of the 4×4 supercell.

The existence of several magnetic configurations competing in energy and the high sensitivity to structural parameters point towards a system with a very large magnetic susceptibility. These wavelike solutions can be fully stabilized if a chemical perturbation is introduced. As an example, we show in Fig. 2(b) a schematic representation of the Nb magnetic pattern obtained for a 4×4 supercell of NbS_2 with a single Fe atom adsorbed on the monolayer. Similar solutions are obtained by substitutional doping with, for instance, Co or Fe vacancies or through other adsorbed species. Small changes in the atomic positions or lattice constants, or the introduction of the spin-orbit interaction, do not destroy the magnetic patterns. The configuration is similar to the one in Fig. 2(a), corresponding to the pristine monolayer. However, unlike the later case, the wavelike configurations are energetically far more favored than the non-SP solution, especially if the defect introduces unpaired bonds or a magnetic moment in the monolayer. For example, the energy differences in the 4×4 supercell are of around 5 meV/Nb for a substitution of Nb by Fe or Co, of 25 meV/Nb for an Nb vacancy, and of 38 meV/Nb for the Fe adsorbtion in Fig. 2(b).

If the hexagonal symmetry of the monolayer is broken by making an infinite line of defects or considering quasi-1D ribbons, the magnetic oscillations occur along a single direction. In Fig. 3(b), we show the obtained magnetic moments of the individual Nb atoms across NbS_2 zigzag ribbons, in the relaxed and unrelaxed structures of equal width. The zigzag cut of the ribbon is presented in Fig. 3(a); on top, the lattice primitive vectors of the monolayer in real and reciprocal space are shown. If the zigzag edge is taken parallel to $\mathbf{a_1}$, then the width N is defined as the number of formula units in the ribbon primitive cell in the direction perpendicular to $\mathbf{a_1}$. Successive rows of Nb atoms are then numbered starting on the Nb-terminated edge. The magnetic moments in Fig. 3(b) correspond to ribbons with $N = 20$. The wavy pattern is also present in ribbons of smaller width (shown in Ref. [8]); however the periodic character is clearer for large N due to a less important finite-size effect. As in the case of the monolayers with point defects, these magnetic solutions are very robust and appear in both the relaxed and unrelaxed cases. Despite their low dimensionality, the NbS_2 ribbons are structurally very rigid. Relaxation affects mainly the positions of the edge atoms (rows 1 and 20), changing their magnetization. The difference in the wavelength of the pattern is due to the slightly smaller lattice constant of the relaxed ribbon. When the SO coupling is considered, the oscillations have a slightly larger amplitude. We note that, as in the monolayer case, this pattern is stabilized by a magnetic perturbation, namely, the ribbon edges. If the edge magnetism is removed, the wavelike configuration disappears. In order to

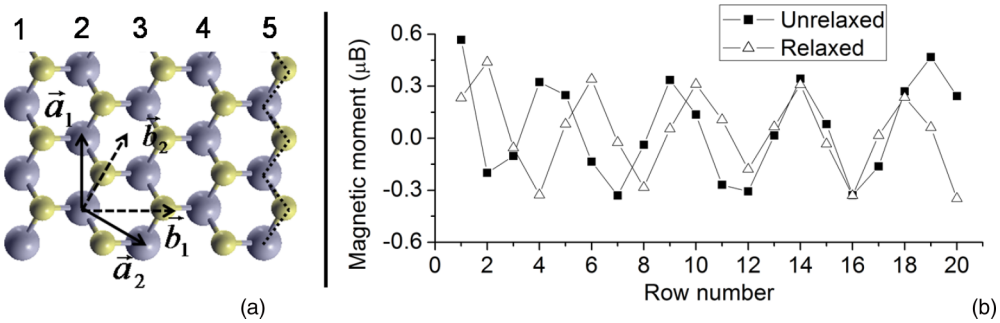

FIG. 3. (a) Top view of the NbS_2 zigzag ribbon structure. Large spheres stand for transition metal atoms, small spheres for chalcogen atoms. The real space ($\mathbf{a_{1,2}}$) and reciprocal space ($\mathbf{b_{1,2}}$) lattice vectors of the NbS_2 monolayer are explicitly plotted. The ribbons are periodic in the $\mathbf{a_1}$ direction and the corresponding edge is marked by the dashed line. Rows of Nb atoms are numbered consecutively, starting on the Nb-terminated edge. (b) Magnetic moments of the individual Nb atoms across the unrelaxed and relaxed NbS_2 zigzag ribbons of width $N = 20$, without SO.

confirm this, we performed calculations on ribbons with edges passivated by hydrogen (not shown). Similarly to the better known case of MoS_2 zigzag ribbons [22], H passivation of all dangling bonds removes the edge magnetism and, in the NbS_2 ribbon, the wavelike pattern as well.

The fact that the wavelike magnetic patterns are present in the unrelaxed perturbed systems is indicating that the magnetic state is of purely electronic origin. We claim that these magnetic patterns are actually SDW instabilities of the NbS_2 monolayer that are stabilized by magnetic point defects or ribbon edges. In order to get insight into the microscopic origin of these magnetic instabilities, we calculate the real part of the bare electronic susceptibility in the static limit and constant matrix approximation [9], $\chi_0'(\mathbf{q})$, and the nesting function, $N_f(\mathbf{q})$, for the NbS_2 monolayer. The real part of the susceptibility reads $\chi_0'(\mathbf{q}) = \sum_{\mathbf{k}} \frac{f_{\mathbf{k}+\mathbf{q}} - f_{\mathbf{k}}}{\epsilon_{\mathbf{k}} - \epsilon_{\mathbf{k}+\mathbf{q}}}$, where $f_{\mathbf{q}}$ is the Fermi function and $\epsilon_{\mathbf{k}}$ is the band energy. In the case of the monolayer, only one band crosses the Fermi level, so that the band index is omitted. The interband contributions in this case do not affect the shape of $\chi_0'(\mathbf{q})$.

In the simplest case, where there is no periodic lattice distortion, the SDW becomes stable when the criterion $\chi_0'(\mathbf{q}) \cdot V_{\mathbf{q}} > 1$ is met, $V_{\mathbf{q}}$ being the exchange matrix element interaction in the local approximation [9]. The orientation of the SDW is given by the direction of $\mathbf{q}$ in real space, and its period by $2\pi/|\mathbf{q}|$. The amplitude of the SDW and the energy gained by the system are determined by the product $\chi_0'(\mathbf{q})\,.\,V_q$. If $V_{\mathbf{q}}$ changes slowly in reciprocal space, a SDW will occur at the wave vector $\mathbf{q}$ for which $\chi_0'(\mathbf{q})$ is maximum, provided the mentioned criterion is satisfied. The imaginary part of the susceptibility, $\chi_0''(\mathbf{q})$, gives information on the nesting properties. It is related to the so called nesting function $N_f(\mathbf{q}) = \lim_{\omega->0} \frac{\chi_0''(\mathbf{q})}{\omega} = \sum_k \delta(\epsilon_F - \epsilon_{\mathbf{k}})\delta(\epsilon_F - \epsilon_{\mathbf{k}+\mathbf{q}})$, where ϵ_F is the Fermi level.

In Fig. 4 we show the calculated $\chi_0'(\mathbf{q})$ for the NbS_2 monolayer in the full first Brillouin zone. The susceptibility has several local maxima for different $\mathbf{q}$ vectors. The highest maximum is found at $\mathbf{q_n} \approx 0.2\mathbf{b_1} = (0.2,0)4\pi/\sqrt{3}a$ and its symmetry equivalent vectors. In Fig. 5, we show the calculated $\chi_0'(\mathbf{q})$ and $N_f(\mathbf{q})$ along the high-symmetry directions Γ-M-K-Γ. The most relevant feature to note from this plot is that the nesting vector for which $N_f(\mathbf{q})$ is maximum is $\mathbf{q_n}$. It matches with the one that maximizes $\chi_0'(\mathbf{q})$; both are indicated with arrows in the plot. We note that the calculated $\chi_0(\mathbf{q})$ depends weakly on the calculation settings and structural parameters being, in fact, very similar to the ones obtained for the undistorted $NbSe_2$ and $TaSe_2$ monolayers (without SO) [12]. When the SO coupling is included, the band crossing ϵ_F splits, giving rise to a concomitant splitting at $\mathbf{q_n}$ in N_f and a slight broadening in $\chi_0'(\mathbf{q})$.

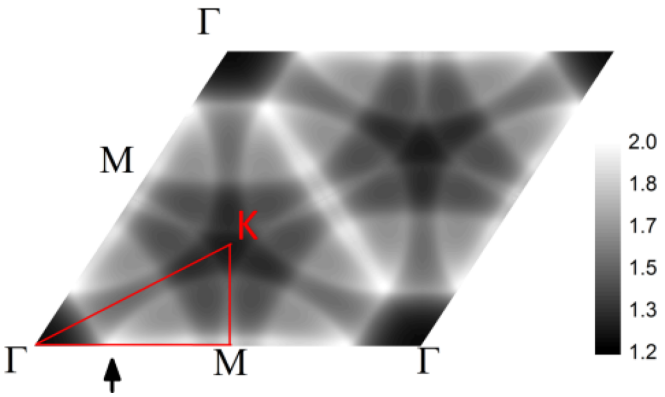

FIG. 4. Real part of the static noninteracting susceptibility $\chi_0'(\mathbf{q})$ of the NbS_2 monolayer (non-SP) in the full first Brillouin zone, without SO. Values are in 1/eV. The arrow points out the absolute maximum, which is along the ΓM direction. The red line marks the edges of the irreducible Brillouin zone.

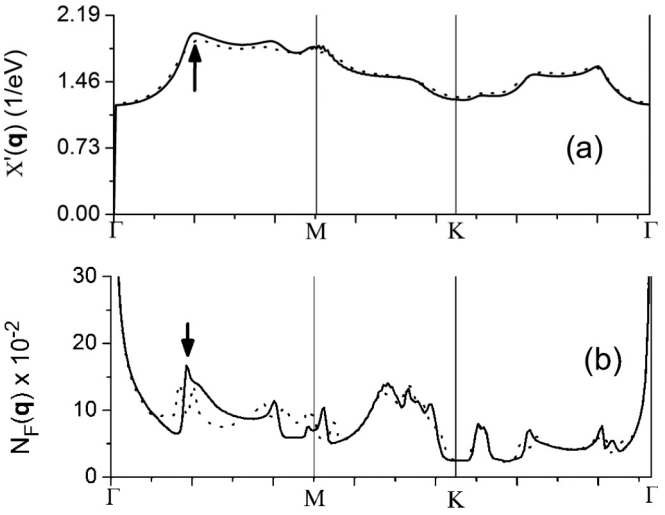

FIG. 5. (a) Real part of the static noninteracting susceptibility $\chi_0'(\mathbf{q})$ and (b) nesting function $N_f(\mathbf{q})$ of the NbS_2 monolayer along the $\Gamma M K \Gamma$ path, with (dashed) and without (solid) SO. The arrows indicate the absolute maximum of $\chi_0'(\mathbf{q})$.

The direction of the magnetic wave pattern shown in Fig. 3(b) is exactly the direction of $\mathbf{q_n}$, which is perpendicular to the ribbon edge [see Fig. 3(a)]. We estimate the wavelength of the resulting SDW from a least-squares fit of the magnetic moments obtained for the NbS_2 nanoribbon of $N = 20$ (by considering 12 innermost rows only). We get $\lambda = 13.88$ Å and $\lambda = 13.43$ Å for the unrelaxed and relaxed cases, respectively. Both values are very close (within 4% and 8%, respectively) to the wavelength corresponding to $\mathbf{q_n}$. It is expected that for ribbons with larger widths, the outcoming λ's should be even closer to $2\pi/|\mathbf{q_n}|$. The magnetic patterns of the monolayer [Fig. 2(a)] should also approach this wavelength if a supercell larger than 4×4 is considered.

In view of this analysis we claim that the wavelike patterns obtained for the doped NbS_2 monolayers and ribbons are SDWs originating in the nesting of the 2D Fermi surface. In the presence of SDWs the NbS_2 monolayer remains metallic. The competing SDW phase presents a partial band splitting, while several dispersive bands still cross ϵ_F.

It is important to remark that besides the high susceptibility and ribbon edges, or other perturbations, a SDW will not be stable in a given system if $V_{\mathbf{q}}$ is not large enough. To show an example of such a situation, we study the magnetic configuration of the TaS_2 zigzag ribbon with $N = 20$. The exchange interaction in $4d$ metals (such as Nb) is stronger than in the $5d$ elements such as Ta, due to the stronger spatial

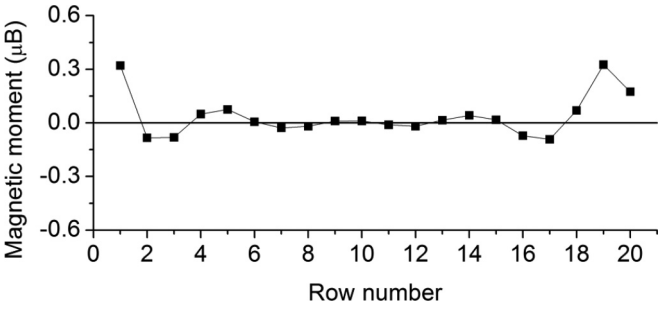

FIG. 6. Magnetic moments of the individual Ta atoms across the TaS_2 zigzag ribbon of width $N = 20$, unrelaxed (without SO). Rows of Ta atoms are numbered consecutively starting on the Ta-terminated edge.

localization of the d orbitals with smaller quantum principal number. In Fig. 6 we present the magnetic moments of the individual Ta atoms in the ribbon. Although there is a wavelike pattern, the oscillation decays rapidly towards the center. In this system the SDW is weaker. We alert the reader that the data of Fig. 6 correspond to an unrelaxed ribbon, without SO, merely used as a way to demonstrate the importance of the exchange interactions in the strength of SDW phases. The actual, physical TaS_2 zigzag ribbon may be subject to CDW phases and stronger SO effects.

It is well known that DFT calculations in their local spin density approximation (LSDA) or in the gradient-corrected GGA overestimate the tendency towards long-range magnetic order in systems that are close to a quantum critical transition. The main reason behind this is the underestimation of quantum fluctuations in LSDA or GGA functionals, these fluctuations being particularly important in critical systems. Recently, an assessment of the magnitude of the spin fluctuations beyond LSDA or GGA calculations has been made for a prototypical critical material as Pd [23], and even more recently, for the ferromagnetic-paramagnetic transition of Ni_3Al under pressure [24]. We propose that the NbS_2 monolayer is close to a quantum critical transition as well. A way to calculate the intensity of the zero-point spin fluctuations is through the fluctuation-dissipation theorem that reads

$$\xi^2 = \frac{2\hbar}{\Omega}\int d^3q \int \frac{d\omega}{2\pi}\mathrm{Im}\chi(\mathbf{q},\omega), \qquad (1)$$

where ξ is the deviation of the spin density from its mean-field value, Ω is the Brillouin zone area, and $\chi(\mathbf{q},\omega)$ the dynamical susceptibility of the pristine NbS_2 monolayer.

Due to the complexity of getting the full dynamical susceptibility, in particular within a first-principles material-specific approach, it is usual to do approximations. One way to estimate ξ is to consider in Eq. (1) the noninteracting $\mathrm{Im}\chi_0(\mathbf{q},\omega) = \sum_{\mathbf{k}}[f(\epsilon_{\mathbf{k}}) - f(\epsilon_{\mathbf{k}+\mathbf{q}})]\delta(\epsilon_{\mathbf{k}+\mathbf{q}} - \epsilon_{\mathbf{k}} - \hbar\omega)$. Here, $\epsilon_{\mathbf{k}}$ are the Kohn-Sham eigenvalues as before [25]. When introducing $\mathrm{Im}\chi_0(\mathbf{q},\omega)$ in Eq. (1), we get $\xi = 0.2\ \mu_B$. This value is an underestimation of the quantum fluctuations of the system, since an enhancement of the spin fluctuations is expected when considering the scattering of the electron-hole pairs due to all the electron-electron interactions [26]. In spite of this, the obtained value for ξ is still quite large, within the same order of magnitude as the calculated static magnetic moments of the magnetic configurations that compete in energy with the nonmagnetic one. We conclude that the spin fluctuations can mitigate the long-range magnetic instabilities in the pristine NbS_2 monolayer but, as shown before, they can be stabilized with doping, impurities, defects, or edges.

It is worth noting that similar values for the static magnetic moments and the fluctuations (ξ) were obtained for Pd by using GGA for the exchange-correlation functional [23] and these fluctuations (paramagnons) were recently detected through inelastic neutron scattering experiments [27].

IV. FURTHER DISCUSSION AND CONCLUSIONS

In this work we have studied, by means of first-principles calculations, the magnetic properties of the NbS_2 monolayer. We have shown that this system presents a high magnetic susceptibility, large spin fluctuations, and is on the verge of a SDW phase. We have also shown that the SDW states can be stabilized either by doping, defects, impurities, or ribbon edges. The physical mechanism behind the SDWs is of pure electronic origin driven mainly by the nesting properties of this two-dimensional material and a rather strong Coulomb interaction in the $4d$ band of the Nb atoms.

Even if no long-range magnetic order has been experimentally observed in NbS_2, either in bulk, thin films, or the monolayer, as far as we know, there are no reported experimental works investigating the spin fluctuations of these systems. Since our results indicate that the monolayer is close to a quantum critical magnetic transition, these kinds of measurements become highly desired.

On the other hand, bulk NbS_2 shows a superconducting phase below $T = 6$ K with similar characteristics to its analogous $2H$-$NbSe_2$. In this last case, the system does show an ordered phase (CDW) whose connection with the superconducting one is still under debate. Although there has been no suggestion other than the electron-phonon coupling for the pairing mechanism of the superconductivity in the TMDC family [4,28], it is difficult to avoid making a conjecture regarding a possible connection of the SDW instabilities predicted in this work and the superconductivity in NbS_2. However, this issue deserves further studies and it is beyond the scope of this paper.

ACKNOWLEDGMENTS

The authors belong to the Institute of Nanoscience and Nanotechnology (INN) of the Atomic Energy Agency (CNEA), Argentina. They acknowledge financial support from ANPCyT (PICT-2011-1187) and CONICET (PIP00069). F.G. and V.L.V. contributed equally to this work.

[1] M. D. Johannes, I. I. Mazin, and C. A. Howells, Phys. Rev. B **73**, 205102 (2006).

[2] M. D. Johannes and I. I. Mazin, Phys. Rev. B **77**, 165135 (2008).

[3] J. Laverock, D. Newby, Jr., E. Abreu, R. Averitt, K. E. Smith, R. P. Singh, G. Balakrishnan, J. Adell, and T. Balasubramanian, Phys. Rev. B **88**, 035108 (2013).
[4] M. Leroux, M. Le Tacon, M. Calandra, L. Cario, M-A. Measson, P. Diener, E. Borrissenko, A. Bosak, and P. Rodiere, Phys. Rev. B **86**, 155125 (2012).
[5] R. A. Klemm, Physica C **514**, 86 (2015).
[6] J. E. Hirsch, M. B. Maple, and F. Marsiglio, Physica C **514**, 1 (2015).
[7] X. Xi, L. Zhao, Z. Wang, H. Berger, L. Forró, J. Shan, and K. F. Mak, Nat. Nanotechnol. **10**, 765 (2015).
[8] F. Güller, V. Vildosola, and A. M. Llois, IEEE Trans. Magn. **49**, 4538 (2013).
[9] S. K. Chan and V. Heine, J. Phys. F: Metal. Phys. **3**, 795 (1973).
[10] M. Calandra, I. I. Mazin, and F. Mauri, Phys. Rev. B **80**, 241108 (2009).
[11] C. Battaglia, H. Cercellier, F. Clerc, L. Despont, M. G. Garnier, C. Koitzsch, P. Aebi, H. Berger, L. Forro, and C. Ambrosch-Draxl, Phys. Rev. B **72**, 195114 (2005).
[12] Y. Ge, Ph.D. thesis, Georgetown University, 2013.
[13] S. Sharma, L. Nordström, and B. Johansson, Phys. Rev. B **66**, 195101 (2002).
[14] G. Kresse and J. Hafner, Phys. Rev. B **47**, 558 (1993).
[15] G. Kresse and J. Furthmüller, Phys. Rev. B **54**, 11169 (1996).
[16] VASP specific settings: PAW pseudopotentials with atomic valence configurations $3s^2 3p^4$ for S, $4s^2 4p^6 4d^4 5s^1$ for Nb, and $5p^6 5d^3 6s^2$ for Ta. Plane wave cutoff: ENCUT = 550 eV. Energy cutoff for self-consistent iterations: EDIFF = 10^{-5} eV. Brillouin zone integration: second-order Methfessel-Paxton with SIGMA = 0.18.
[17] P. Blaha, K. Schwarz, G. K. H. Madsen, D. Kvasnicka, and J. Luitz, *WIEN2k, An Augmented Plane Wave + Local Orbitals Program for Calculating Crystal Properties* (Technische Universität, Wien, Austria, 2010).
[18] WIEN2k specific settings: the muffin tin radii used were 1.2 au for S and 2.0 au for Nb and Ta. Plane wave cutoff: RKMAX = 8. Energy and charge distance cutoff for self-consistent iterations: 10^{-4} Ry and $10^{-4}e$, respectively.
[19] J. P. Perdew, K. Burke, and M. Ernzerhof, Phys. Rev. Lett. **77**, 3865 (1996).
[20] P. Raybaud, G. Kresse, J. Hafner, and H. Toulhoat, J. Phys.: Condens. Matter **9**, 11085 (1997).
[21] The difference in the value of the zc parameter is most likely due to the van der Waals interactions between layers, which are absent when a single monolayer is considered, but are present in the bulk.
[22] A. R. Botello-Méndez, F. López-Urías, M. Terrones, and H. Terrones, Nanotechnol. **20**, 325703 (2009).
[23] P. Larson, I. I. Mazin, and D. J. Singh, Phys. Rev. B **69**, 064429 (2004).
[24] L. Ortenzi, I. I. Mazin, P. Blaha, and L. Boeri, Phys. Rev. B **86**, 064437 (2012).
[25] The calculated χ_0 is not exactly *noninteracting* because we use the GGA eigenvalues. It is usually called this in the literature and we continue with this terminology.
[26] T. Moriya, *Spin Fluctuations in Itinerant Electron Magnetism* (Springer, Berlin, 1985).
[27] R. Doubble, S. M. Hayden, Pengcheng Dai, H. A. Mook, J. R. Thompson, and C. D. Frost, Phys. Rev. Lett. **105**, 027207 (2010).
[28] M. Calandra and F. Mauri, Phys. Rev. Lett. **106**, 196406 (2011).